



Published in final edited form as:

J Thorac Cardiovasc Surg. 2013 January ; 145(1): 285–293.e2. doi:10.1016/j.jtcvs.2012.03.009.

Using Contracting Band to Improve Right Ventricle Ejection Fraction for Patients with Repaired Tetralogy of Fallot, a Modeling Study Using Patient-Specific CMR-Based Two-Layer Anisotropic Models of Human Right and Left Ventricles

Chun Yang^{1,2}, Dalin Tang^{1,*}, Tal Geva³, Rahul Rathod³, Haruo Yamauchi⁴, Vasu Gooty³, Alexander Tang³, Glenn Gaudette⁵, Kristen L. Billiar^{5,6}, Mehmet H. Kural⁵, and Pedro J. del Nido⁴

¹Mathematical Sciences Department, Worcester Polytechnic Institute, Worcester, MA 01609

²School of Mathematical Sciences, Beijing Normal University, Key Laboratory of Mathematics and Complex Systems, Ministry of Education, Beijing, 100875, China

³Dept of Cardiology, Children's Hospital Boston, Dept of Pediatrics, Harvard Medical School, Boston, MA 02115 USA

⁴Dept. of Cardiac Surgery, Children's Hospital Boston, Dept of Surgery, Harvard Medical School, Boston, MA 02115 USA

⁵Dept of Biomedical Engineering, Worcester Polytechnic Institute, MA 01609, USA

⁶Department of Surgery, University of Massachusetts Medical School, Worcester, MA 01655

Abstract

Objectives—Patients with repaired tetralogy of Fallot (TOF) account for the majority of cases with late onset right ventricle (RV) failure. The current surgical approach, which includes pulmonary valve replacement/insertion (PVR), has yielded mixed results. A new surgical option placing an elastic band in the right ventricle is proposed to improve RV cardiac function measured by ejection fraction (EF).

Methods—A total of 20 computational RV/LV/Patch/Band combination models based on cardiac magnetic resonance (CMR) imaging from a TOF patient were constructed to investigate the impact of band material stiffness variations, band length and active contraction. These models included 4 different band material properties, 3 band length, three active contracting band materials, and models with patch and scar replaced by contracting tissues.

Results—Our results indicate that the band insertion, combined with active band contraction and tissue regeneration techniques that restore RV myocardium, has the potential to improve right ventricle ejection fraction by 7.5% (41.63% EF from the best active band model over 34.10% EF from baseline passive band model) and 4.2% (41.63% from the best active band model over CMR-measured EF 37.45%).

© 2012 The American Association For Thoracic Surgery. Published by Mosby, Inc. All rights reserved.

*Corresponding author: Dalin Tang, Ph.D., FAHA, Mathematical Sciences Department, Worcester Polytechnic Institute, Worcester, MA 01609, dtang@wpi.edu, Phone: 508-831-5332, fax: 508-831-5824.

Publisher's Disclaimer: This is a PDF file of an unedited manuscript that has been accepted for publication. As a service to our customers we are providing this early version of the manuscript. The manuscript will undergo copyediting, typesetting, and review of the resulting proof before it is published in its final citable form. Please note that during the production process errors may be discovered which could affect the content, and all legal disclaimers that apply to the journal pertain.

Conclusion—The CMR-based RV/LV/Patch/Band model provides a “proof of concept” for using elastic bands to improve RV cardiac function. The band insertion combined with myocardium regeneration techniques and RV remodeling surgical procedures has the potential to improve ventricular function in patients with repaired TOF and other similar forms of RV dysfunction after surgery. Further investigations using in vitro experiments, animal models and final patient studies are warranted.

Keywords

Right ventricle; congenital heart disease; heart model; Dacron scaffold patch; fluid-structural interaction

1 Introduction

Patients with repaired Tetralogy of Fallot (ToF), a congenital heart defect which includes a ventricular septal defect and severe right ventricular outflow obstruction, account for the majority of cases with late onset RV failure. The current surgical approach, which includes pulmonary valve replacement/insertion (PVR), has yielded mixed results with many patients not recovering RV function after pulmonary valve insertion with or without concomitant RV remodeling surgery [1–3]. Recent advances in computational modeling, methods and computer technology have made it possible for computer-simulated procedures to be used in clinical decision-making process to replace empirical and often risky clinical experimentation to examine the efficiency and suitability of various reconstructive procedures in diseased hearts [4–16]. Peskin pioneered heart modeling effort with his celebrated immersed boundary method [4–5]. More recently, Hunter, McCulloch, Guccione, Kerckhoffs, Costa, Axel, Saber and many other authors have made great contributions to passive and active ventricle modeling, including the Physiome Project and the Continuity package [6–13]. Early MRI-based ventricle models were introduced by Axel and Saber et al. for mechanical analysis and investigations [12–13]. In our previous papers, patient-specific cardiac magnetic resonance (CMR) image-based computational right and left ventricle (RV/LV) models with fluid-structure interactions were introduced to assess outcomes of various RV reconstruction techniques with different scar tissue trimming and patch sizes [14–16]. A recent review can be found in [14].

For patients with ToF who need PVR surgery, surgical intervention such as scar tissue resection and anterior wall RV remodeling have been proposed in order to improve RV function recovery [17]. The RV remodeling aims mainly to reduce RV volume by removing or reducing the non-contracting tissue (scar and patch) in the outflow area of the RV (see Fig. 1). In our clinical trial, 64 patients who underwent RV outflow tract procedures in early childhood had more than or equal to moderate pulmonary regurgitation, and fulfilled defined criteria for PVR were randomly assigned to undergo either PVR alone (n=34) or PVR with surgical RV remodeling (n=30). However, no significant difference was observed in the primary outcome (change in RV ejection fraction, $-2\pm 7\%$ in the PVR alone group vs. $-1\pm 7\%$ in the PVR with RV remodeling group; $P=0.38$) or in any of the secondary outcomes at 6-month postoperative follow-up [18]. We are currently attempting to identify factors which may help us to identify patients who would benefit from the PVR remodeling procedures via a sub-analysis [16].

In this paper, in our continuous effort seeking new surgical options for better RV function recovery, we have utilized our mathematical models of the late post-operative RV to evaluate the impact of novel interventions. To this end, we have introduced the concept of an elastic band with varying elastic properties and also the capacity for active force generation similar to normal myocardium. This band concept was added to our previous

patient-specific MRI-based RV/LV/Patch models to investigate its impact and potential improvement on RV cardiac function and mechanical performance. The band models included (a) an elastic band connecting the RV anterior free wall and the septum; (b) two-layer ventricle myocardial wall construction with realistic epicardial and endocardial fiber orientations, replacing the previous RV outflow non-myocardium patch; (c) anisotropic material properties for both RV and LV tissues; (d) a patch/scar area with different materials; (e) LV as support to the RV structure. Since we were mainly concerned with whether addition of the band would lead to improved RV ejection fraction, structure-only models were used, as opposed to our previous models, which included fluid-structure interactions (FSI). A total of 20 models based on MRI studies obtained in patients being evaluated for surgery to treat RV dilation and dysfunction late after ToF repair, were constructed, including 4 different band material properties, 3 band lengths, one passive and three active contracting band materials, and models with patch and scar all replaced by contracting myocardium. The 3D CMR-based RV/LV/Patch/Band models were solved to obtain 3D ventricular deformation and stress/strain distributions for accurate assessment of RV cardiac function and mechanical conditions. The computational models were validated by CMR data first and then used to assess the effect of different band approaches with the ultimate goal of improving recovery of RV function after surgery.

2. Data Acquisition, Models and Methods

2.1 Data acquisition, 3D geometry re-construction and band location

CMR studies were performed by Dr. Tal Geva to acquire patient-specific ventricular geometry for a patients needing RV remodeling and pulmonary valve replacement operations before and after surgery (Fig. 2(a)). The RV and LV were imaged using ECG-gated, breath-hold steady state free precession cine MR in the ventricular short axis (12–14 equidistant slices covering the ventricles from base to apex; slice thickness 6–8 mm; interslice gap 0–2 mm; 30 frames per cardiac cycle). The valve and patch positions were determined with cine MR imaging, flow data, and delayed enhancement CMR to delineate location and extent of scar/patch. The CMR findings were subsequently confirmed by the intra-operative observations (del Nido). Three-dimensional RV/LV geometry and computational mesh were constructed following the procedures described in [14–16]. Figure 2 shows pre-operative CMR images from the patient with repaired TOF and severe RV dilatation, the segmented contour pots, the stacked contours showing the location and orientation of the hypothetic elastic band, and 3D re-construction RV/LV geometry with a front view showing the patch, scar, band and the RV outflow track (RVOT). The location of the band was carefully chosen to help the RV to contract in the present model.

2.2 The anisotropic material models for RV tissues and band, fiber orientation and two-layer model construction

The governing equations for all material models were:

$$\rho v_{i,tt} = \sigma_{ij,j}, \quad i, j = 1, 2, 3; \text{sum over } j, \quad (1)$$

$$\varepsilon_{ij} = (v_{i,j} + v_{j,i} + v_{\alpha,i} v_{\alpha,j}) / 2, \quad i, j, \alpha = 1, 2, 3, \quad (2)$$

where σ is the stress tensor, ε is the strain tensor, \mathbf{v} is displacement, $f_{\bullet,j}$ stands for derivative of f with respect to the j th variable, and ρ is material density. The normal stress was assumed to be zero on the outer RV/LV surface and equal to the normal stress imposed by fluid pressure on the inner RV/LV surfaces. Structure-only RV/LV models were used to save model construction effort and computing time. They were adequate for our purpose in

this paper to obtain RV volume and ejection fractions for ventricle cardiac function assessment.

The RV and LV materials were assumed to be hyperelastic, anisotropic, nearly-incompressible and homogeneous. Band, patch and scar materials were assumed to be hyperelastic, isotropic, nearly-incompressible and homogeneous. The nonlinear Mooney-Rivlin model was used to describe the nonlinear anisotropic and isotropic material properties. The strain energy function for the isotropic modified Mooney-Rivlin model is given by [14,19]:

$$W=c_1(I_1 - 3)+c_2(I_2 - 3)+D_1 [\exp(D_2(I_1 - 3)) - 1], \quad (3)$$

where I_1 and I_2 are the first and second strain invariants given by,

$$I_1 = \sum C_{ii}, \quad I_2 = \frac{1}{2} [I_1^2 - C_{ij}C_{ij}], \quad (4)$$

$C = [C_{ij}] = X^T X$ is the right Cauchy-Green deformation tensor, $X = [X_{ij}] = [x_i/a_j]$, (x_i) is the current position, (a_i) is the original position, c_1 and D_1 are material parameters chosen to match experimental measurements [14,20–21]. The strain energy function for the anisotropic modified Mooney-Rivlin model anisotropic model was obtained by adding an additional anisotropic term in Eq. (3) [19,22]:

$$W=c_1(I_1 - 3)+c_2(I_2 - 3)+D_1 [\exp(D_2 (I_1 - 3)) - 1] + K_1/(2K_2) \exp[K_2(I_4 - 1)^2 - 1], \quad (5)$$

where $I_4 = C_{ij} (\mathbf{n}_f)_i (\mathbf{n}_f)_j$, C_{ij} is the Cauchy-Green deformation tensor, \mathbf{n}_f is the fiber direction, K_1 and K_2 are material constants [19]. A two-step least-squares method was used to determine the parameter values in (5) to fit the experimental data given in [6]. Step 1: With D_2 and K_2 fixed, least square approximation technique was used to obtain C_1 , D_1 , K_1 (all dependent on D_2 and K_2) so that the stress-strain curves in the fiber and circumferential directions derived from Eq. (5) have minimum error (best match) with experimental data. Step 2: Let D_2 and K_2 change from -100 to 100 , we perform Step 1 to get the corresponding C_1 , D_1 , K_1 values, and the fitting error for all (D_2 , K_2) combinations with initial increment=10. Optimal (D_2 , K_2) and the associated C_1 , D_1 , K_1 values are determined by choosing the pair corresponding to a minimum error. Searching increment for (D_2 , K_2) starts from 10 for $[-100,100]$ and then refines to 1, and 0.1 when the search domain is reduced. Even though the procedure involves a huge number of calculations, it is fully automatic and can be used to find the best fit for any measured experimental data. Choosing $c_1=0.351$ KPa, $c_2=0$, $D_1=0.0633$ KPa, $D_2=5.3$, $K_1=1.913$ KPa, $K_2=6.00$, it was shown [14–15] that stress-strain curves derived from Eq. (5) agreed very well with the stress-strain curves from the dog model given in [6]. Parameter values were then adjusted to fit CMR-measured RV volume data. The stress-stretch curves and parameter values of the RV/LV tissues, patch, scar and band are given in Fig. 3. Imposed RV pressure conditions and computational RV volume data from our baseline no-band model were given in Fig. 3(c)–(d). Good agreement between computational and CMR-measured volume data was found (error < 2%).

For the elastic band model, uniaxial mechanical testing was performed using three sample bands made of Tecoflex EG-80A (Lubzizol Advanced Materials, Inc., Cleveland, Ohio, USA) to obtain material parameter values for our band material. The stress-stretch curves from Mooney-Rivlin model fitting ME test data of the Tecoflex band and 5 other materials are shown in Fig. 3(b).

Three active band contraction models (with 10%, 15% and 20% band zero-stress length reduction) were evaluated to measure improvements if any, in RV EF. “Actively contracting band” should be made of material which is able to contract the same way as normal myocardium does. This paper is mainly to demonstrate the potential benefit of actively contracting bands if such materials could be made available. Active band contraction was achieved by using an iterative procedure and coupling a separate simple band-only model to the whole RV/LV/Patch/Band model to adjust band zero-stress length (contraction at the start of systole and relaxation at the start of diastole), re-calculate band displacement, stress and strain using the band-only model, and assign the displacement, stress and strain values to the band in the right ventricle as the start for the whole model with a new zero-stress band length.

As patient-specific fiber orientation data was not available in practice, we chose to construct a two-layer RV/LV model and set fiber orientation angles using fiber angles given in Hunter et al. [8] (see Fig. 4). Fiber orientation can be adjusted when patient-specific data becomes available [23]. Figure 4 shows ventricular fiber orientations on epicardium and endocardium layers from human and a pig hearts and how the two-layer RV/LV model was constructed [8,14,23].

2.3 Mesh generation: a pre-shrink process and geometry-fitting technique for patient-specific CMR-based models

Under the *in vivo* condition, the ventricles were pressurized and the zero-stress ventricular geometries were not known. In our model construction process, a pre-shrink process was applied to the *in vivo* end-systolic ventricular geometries to generate the starting shape (zero ventricle pressure) for the computational simulation. The initial shrinkage for the inner ventricular surface was 2–3% and end-systolic pressure was applied so that the ventricles would regain its *in vivo* morphology. The outer surface of the ventricular shrinkage was determined by conservation of mass so that the total ventricular wall mass was conserved. Without this shrinking process, the actual computing domain would be greater than the actual ventricle due to the initial expansion when pressure was applied.

Because ventricles have complex irregular geometries with patch and scar tissue component inclusions which are challenging for mesh generation, a geometry-fitting mesh generation technique was developed to generate mesh for our models. Figure 4(g) gives an illustration of RV/LV geometry between two slices. Each slice was first divided into geometry-fitting areas (called “surfaces” in ADINA). The neighboring slices were stacked to form volumes. Using this technique, the 3D RV/LV domain was divided into many small “volumes” to curve-fit the irregular plaque geometry with patch as an inclusion. For the baseline RV/LV/Patch model constructed in this paper, the ADINA model had 1759 small volumes, 30273 nodes, and 26276 elements. Mesh analysis was performed by decreasing mesh size by 10% (in each dimension) until solution differences were less than 2%. The mesh was then chosen for our simulations.

2.4 The model list, solution methods, and simulation procedures

Twelve models with 4 different material stiffness (1 Stiff, 0.5 Stiff, 0.25 Stiff and 0.05 Stiff, parameter values given in Fig. 3) and 3 different band length (100%, 90% and 80% of original baseline model length) were constructed to evaluate the impact of band material stiffness and length on RV cardiac function commonly measured by its stroke volume (SV) and ejection fraction (EF) which are defined as:

$$SV = \text{RV End Diastolic volume (RVEDV)} - \text{RV End Systolic Volume (RVESV)}; \quad (6)$$

$$EF=[RVEDV - RVESV]/RVEDV. \quad (7)$$

Furthermore, active contraction band models were made by allowing the band to contract 10%, 15%, and 20% to improve EF values. The full RV/LV/Patch/Band models were solved by ADINA (ADINA R&D, Watertown, MA, USA) using unstructured finite elements and the Newton-Raphson iteration method [19]. Stress/strain distributions and RV ejection fraction were calculated to seek the optimal surgical design for potential RV EF improvement.

3. Results

For the patient under consideration, the RV ejection fraction (EF) from our baseline no-band model was 37.48%, in agreement with the EF data (37.45%) from direct CMR measurement. A total of 20 models were made from the baseline model to investigate the impact of material and band length variations, active band contraction, and use of viable tissues replacing the patch and scar.

3.1 Impact of band material stiffness and length on RV ejection fraction (EF)

Table 1 presents a summary of RV ejection fraction from 12 models, with 4 stiffness and 3 band length variations. We started from a fixed Stiffness, which was given a value of “1”, and reduced it incrementally to Stiffness of 0.05 (see Table 1 for parameter values), which is close to the stiffness of the Tecoflex material. The band was made softer with the hope that softer material would have more passive elastic contractions and would lead to better EF. Our results indicated that the addition of a passive elastic band led to about 5% EF reduction for all the 12 models considered. A softer band provided slightly better ejection fraction (EF was 1.5% higher). Band length had very little effect on EF.

3.2 Impact of active band contraction on RV ejection fraction (EF)

Since passive band materials led to lower EF rates, three active contractions (band zero-stress length reduced by 10%, 15% and 20%) were added to the band seeking possible RV EF improvements. Table 2 shows the EF values from the three active band models (ABM1-ABM3) for RV with patch and scar improved from 34.10% (PBM13, the corresponding passive band model) to 37.43%, 39.39%, and 39.92%, respectively. The EF improvement from PBM13 to ABM3 was 5.62%. When the patch and scar were replaced by “normal RV tissue”, i.e. the scar area was replaced by myocardial tissue with normal contractile properties, the EF values from the three active band models (ABM4-ABM6) improved from 35.59% (PBM14, the corresponding passive band model) to 39.54%, 40.99%, and 41.63%, respectively. The EF improvement from PBM14 to ABM6 was 6.04%.

3.3 Stress/strain distributions have complex patterns in the ventricle

Figure 5 (online figure) 11 shows the inner RV surface viewed from one cut plane, the corresponding maximum principal stress (Stress- P_1) and strain (Strain- P_1) plots from three selected models: (a) baseline model with patch and scar, no band; (b) Passive band model with patch and scar; (c) Passive band model with patch and scar replaced by normal tissue. Some mesh lines were kept to show the 3D surface better. Clearly the RV geometry, curvature, material properties, patch, scar and band all have considerable contributions to RV stress/strain distributions. Large curvature caused noticeable stress/strain concentrations in all three models. High stress/strain concentrations were also found where the band was connected to RV. Replacing patch and scar by normal tissue led to smoother stress/strain

distributions. This could become possible if and when viable myocardium tissues could be generated using tissue engineering techniques under development [24–25].

4. Discussion

4.1. Motivation to develop the band model and clinical potential

With the rapidly increasing number of late survivors of Tetralogy of Fallot repair, surgical management of patients with right ventricular dysfunction has become a major clinical challenge. The wide variability in clinical status, regurgitation at both tricuspid and pulmonary valves, extent of right ventricular dilatation, scarring, and dysfunction at the time of presentation has resulted in disparate surgical results with pulmonary valve insertion alone [3]. del Nido and Geva et al. have proposed aggressive scar tissue removal and RV volume remodeling as a way to improve RV function after pulmonary valve replacement surgery [17]. However, in a randomized prospective clinical trial, this aggressive approach did not result in measurable improvement in RV ejection fraction or RV end-diastolic volume compared to pulmonary valve insertion and RVOT patch reduction alone. The current proposed band approach is another approach to assist the ventricle to contract and improve its EF. If an active contracting material or actuator could be used for the band material, the band may be able to augment the contraction of the RV. Proulx et al. described a band made from fibrin that could be seeded with mesenchymal stem cells and stitched through a collagen gel [26]. Seeding these fibrin bands with contractile cells, possibly derived from stem cells, may provide an actively contracting band. Also, recent work suggests that contractile cells can be generated to replace scarred myocardium, providing a contracting scaffold [24–25]. Combined with the tissue regeneration techniques that restore RV myocardium, the combined scar tissue replacement plus active band approach has the potential to improve ejection fraction by 7.5% (41.63% from best active band model ABM6 over 34.10% from passive band model PBM13) and 4.2% (41.63% from ABM6 over 37.45% from CMR EF data). The percentage increase in ejection fraction is significant, representing a 22% relative improvement over the observed EF of 34%. The impact on functional status will depend on a number of factors such as LV function. However, a 7% increase in RVEF compares favorably with recently published drug trials to treat heart failure where an improvement in LVEF of 3–4% resulted in a significant improvement in functional capacity [27].

The computational simulations (virtual surgery) provided “proof of concept” for further investigations using in vitro experiments, animal models and final patient studies. Computational models are non-invasive and may be used to supplement/replace empirical and often risky clinical experimentation, or even guide the design of new clinical trials to examine the efficiency and suitability of various reconstructive procedures in diseased hearts.

4.2. Passive RV band and tricuspid regurgitation

Similar passive ventricular restriction approaches to the one proposed here have been evaluated and implanted in patients with left ventricular dilation and functional mitral regurgitation. An example of this approach is the Coapsys device (Myocor, Maple Grove, MN, USA). As the Coapsys device demonstrated effectiveness in reducing not only functional mitral regurgitation but also short-axis LV dimensions [28], the proposed RV band approach may also be expected to improve RV dimensions and may even be effective in treating functional tricuspid regurgitation, which is seen in these patients. Considering that annular and ventricular dilatation contributes to tricuspid regurgitation, the passive band may be effective in reducing regurgitation, even though the passive band had little effect on EF in the present study.

4.3. Mechanical analysis and its relevance to ventricular remodeling, myocardial regeneration, and surgical design

It is well known that mechanical forces play an important role in biological processes. Peskin, Hunter, McCulloch, Guccione, Costa, Kerchhoffs and other authors have made considerable contributions for ventricle models which serve as foundation for many further development and investigations [4–13]. The *in vivo* MRI-based human RV/LV/Patch/Band model is adding the band into consideration as a potential surgical option for ventricle repair. While the structure-only model is sufficient for our purpose in this paper, fluid-structure-interaction (FSI) models will be developed which will allow us to investigate both flow and structure stress/strain behaviors and their influences on various biological processes, including ventricle remodeling and myocardium regeneration. As we continue our investigations on ventricular remodeling and myocardium tissue regeneration following stem cell seeding, detailed localized mechanical stress and flow conditions will be obtained to quantify their effects and influence on ventricular remodeling, myocardium tissue regeneration, and related cellular activities. Our RV/LV/Patch FSI model can serve as a useful tool to investigate cellular biology and tissue regeneration under localized flow and structural stress environment.

4.4 Model limitations and future directions

Several improvements can be added to our models in the future for better accuracy and applicability: a) multi-band design for better tricuspid valve closure to address the regurgitation issue; b) fluid-structure interaction to obtain both flow and structural stress/strain information for complete mechanical analysis; c) direct measurements of tissue mechanical properties for improved accuracy of our models; d) proper ways to model active contraction by adding active stress and techniques adjusting zero-stress sarcomere fiber length; e) inclusion of both tricuspid and pulmonary valve mechanics in the model to simulate regurgitation; f) multi-scale models including organ, cell, and gene investigations. This will allow mechanical conditions obtained from organ level to pass to micro level and cell activities obtained from micro level to organ level to discover mechanisms governing tissue regeneration process. Diastolic dysfunction, defined as an abnormal stress-strain relationship when the heart is in a relaxed state was not evaluated in this model, and will be investigated in the future using proper model assumptions and patient data for that purpose.

5. Conclusion

The CMR-based RV/LV/Patch/Band model introduced in this paper provides a “proof of concept” for using passive or actively contracting elastic bands to improve RV cardiac function. The impact of band material stiffness variations, band length and active contraction were investigated. Our preliminary results indicate that the band insertion, combined with active band contraction and tissue regeneration techniques that restore RV myocardium, has the potential to improve right ventricle ejection fraction by 7.5% and 4.2%. The computational simulations suggested that further investigations using *in vitro* experiments, animal models and final patient studies are warranted. The band insertion combined with myocardium regeneration techniques and RV remodeling surgical procedures has promising potential to improve ventricular function in patients with repaired TOF and other congenital heart disease.

Acknowledgments

This research was supported in part by NIH-1R01-HL 089269 (del Nido, Tang, Geva), NIH-HL63095 (PI: del Nido) and NIH-NHLBI 5P50HL074734 (PI: Geva; Co-Investigator: del Nido). Chun Yang’s research is supported in part by National Sciences Foundation of China 11171030 and the Fundamental Research Funds for the Central Universities.

References

1. Therrien J, Siu SC, McLaughlin PR. Pulmonary valve replacement in adults late after repair of tetralogy of Fallot: are we operating too late? *J Am Coll Cardiol*. 2000; 36:1670–5. [PubMed: 11079675]
2. Vliegen HW, Van Straten A, De Roos A, Roest AA, Schoof PH, Zwinderman AH, Ottenkamp J, Van Der Wall EE, Hazekamp MG. Magnetic resonance imaging to assess the hemodynamic effects of pulmonary valve replacement in adults late after repair of tetralogy of Fallot. *Circulation*. 2002; 106:1703–1707. [PubMed: 12270866]
3. Waien SA, Liu PP, Ross BL, Williams WG, Webb GD, McLaughlin PR. Serial follow-up of adults with repaired tetralogy of Fallot. *J Am Coll Cardiol*. 1992; 20:295–300. [PubMed: 1634663]
4. Peskin CS. Numerical analysis of blood flow in the heart. *J Com Phys*. 1977; 25:220–252.
5. Peskin CS. A three-dimensional computational method for blood flow in the heart. *J Comp Physics*. 1989; 81:372–405.
6. McCulloch AD, Waldman L, Rogers J, Guccione JM. Large-scale finite element analysis of the beating heart. *Critical Rev in Biomedical Engineering*. 1992; 20(5,6):427–449.
7. Kerckhoffs RC, Neal ML, Gu Q, Bassingthwaite JB, Omens JH, McCulloch AD. Coupling of a 3D finite element model of cardiac ventricular mechanics to lumped systems models of the systemic and pulmonic circulation. *Ann Biomed Eng*. 2007 Jan; 35(1):1–18. [PubMed: 17111210]
8. Hunter PJ, Pullan AJ, Smaill BH. Modeling total heart function. *Annu Rev Biomed Eng*. 2003; 5:147–77. [PubMed: 14527312]
9. Nash MP, Hunter PJ. Computational Mechanics of the Heart, From tissue structure to ventricular function. *Journal of Elasticity*. 2000; 61:113–141.
10. Costa KD, Takayama Y, McCulloch AD, Covell JW. Lamina fiber architecture and three-dimensional systolic mechanics in canine ventricular myocardium. *Am J Physiol*. 1999; 276(2 Pt 2):H595–607. [PubMed: 9950861]
11. Guccione JM, Waldman LK, McCulloch AD. Mechanics of active contraction in cardiac muscle: Part II--Cylindrical models of the systolic left ventricle. *J Biomech Eng*. 1993; 115(1):82–90. [PubMed: 8445902]
12. Axel L. Biomechanical dynamics of the heart with MRI. *Annu Rev Biomed Eng*. 2002; 4:321–347. [PubMed: 12117761]
13. Saber NR, Gosman AD, Wood NB, Kilner PJ, Charrier CL, Firman DN. Computational flow modeling of the left ventricle based on in vivo MRI data: initial experience. *Annals of Biomech Engng*. 2001; 29:275–283.
14. Tang D, Yang C, Geva T, del Nido PJ. Image-Based Patient-Specific Ventricle Models with Fluid-Structure Interaction for Cardiac Function Assessment and Surgical Design Optimization. *Progress in Pediatric Cardiology*. 2010; 30:51–62. PMC3041970. [PubMed: 21344066]
15. Tang D, Yang C, Geva T, Gaudette G, del Nido PJ. Multi-Physics MRI-Based Two-Layer Fluid-Structure Interaction Anisotropic Models of Human Right and Left Ventricles with Different Patch Materials: Cardiac Function Assessment and Mechanical Stress Analysis. *Computers & Structures*. 2011; 89:1059–1068. PMC3134331. [PubMed: 21765559]
16. Tang D, Yang C, Geva T, del Nido PJ. Patient-specific MRI-based 3D FSI RV/LV/Patch models for pulmonary valve replacement surgery and patch optimization. *J of Biomech Engineering*. 2008; 130(4):041010.
17. del Nido PJ. Surgical management of right ventricular dysfunction late after repair of Tetralogy of Fallot: right ventricular remodeling surgery. *Semin Thorac Cardiovasc Surg Pediatr Card Surg Annu*. 2006:29–34. [PubMed: 16638544]
18. Geva T, Gauvreau K, Powell AJ, Cecchin F, Rhodes J, Geva J, del Nido P. Randomized Trial of Pulmonary Valve Replacement With and Without Right Ventricular Remodeling Surgery. *Circulation*. 2010 Sep 14; 122(11 Suppl):S201–8. [PubMed: 20837914]
19. Bathe, KJ. *Finite Element Procedures*. Prentice Hall, Inc; New Jersey: 1996.
20. Sacks MS, Chuong CJ. Biaxial mechanical properties of passive right ventricular free wall myocardium. *J Biomech Eng*. 1993; 115:202–205. [PubMed: 8326727]
21. Humphrey, JD. *Cardiovascular Solid Mechanics*. Springer-Verlag; New York: 2002.

22. Holzapfel GA, Gasser TC, Ogden RW. A new constitutive framework for arterial wall mechanics and a comparative study of material models. *J of Elasticity*. 2000; 61:1–48.
23. Sanchez-Quintana D, Anderson R, Ho SY. Ventricular myoarchitecture in tetralogy of Fallot. *Heart*. 1996; 76:280–286. [PubMed: 8868990]
24. Kochupura PV, Azeloglu EU, Kelly DJ, Doronin SV, Badylak SF, Krukenkamp IB, Cohen IS, Gaudette GR. Tissue-engineered myocardial patch derived from extracellular matrix provides regional mechanical function. *Circulation*. 2005; 30,112(9 S):1144–9. [PubMed: 16159807]
25. Kelly DJ, Rosen AB, Schuldt AJ, Kochupura PV, Doronin SV, Potapova IA, Azeloglu EU, Badylak SF, Brink PR, Cohen IS, Gaudette GR. Increased myocyte content and mechanical function within a tissue-engineered myocardial patch following implantation. *Tissue Eng Part A*. 2009; 15(8):2189–2201. [PubMed: 19231971]
26. Proulx MK, Carey SP, Ditroia LM, Jones CM, Fakharzadeh M, Guyette JP, Clement AL, Orr RG, Rolle MW, Pins GD, et al. Fibrin microthreads support mesenchymal stem cell growth while maintaining differentiation potential. *J Biomed Mater Res A*. 2011; 96(2):301–12. [PubMed: 21171149]
27. Aleksova A, Masson S, Maggioni AP, Lucci D, Urso R, Staszewsky L, Ciaffoni S, Cacciatore G, Misuraca G, Gulizia M, Mos L, Proietti G, Minneci C, Latini R, Sinagra G. on the behalf of the CandHeart Investigators. Effects of Candesartan on Left Ventricular Function, Aldosterone and BNP in Chronic Heart Failure. *Cardiovasc Drugs Ther*. 2012 Feb 3. [Epub ahead of print].
28. Grossi EA, Woo YJ, Schwartz CF, Gangahar DM, Subramanian VA, Patel N, Wudel J, DiGiorgi PL, Singh A, Davis RD. Comparison of Coapsys annuloplasty and internal reduction mitral annuloplasty in the randomized treatment of functional ischemic mitral regurgitation: Impact on the left ventricle. *J Thorac Cardiovasc Surg*. 2006; 131:1095–8. [PubMed: 16678595]

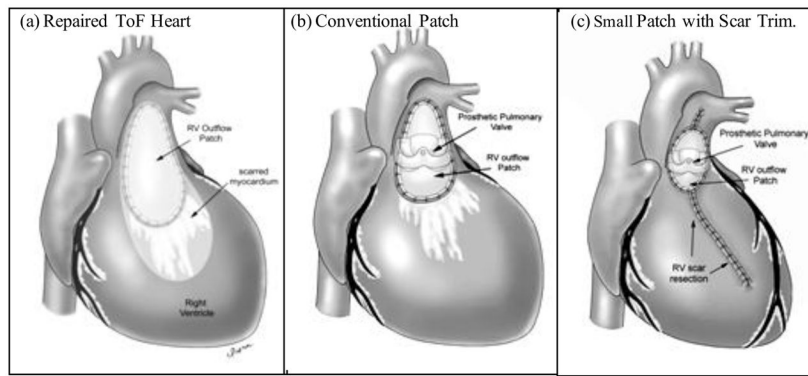


Figure 1.

A hypothesis that smaller patch and removal of RV scar may lead to improved surgical outcome after surgery. (a) Repaired Tetralogy of Fallot heart with RV outflow patch and scar on anterior RV wall. (b) RV after pulmonary valve insertion (PVR) and reduction of RV outflow patch (*current practice*). (c) RV after pulmonary valve insertion (PVR), reduction of RV outflow patch and removal of RV scar (RV remodeling, proposed new surgical procedure).

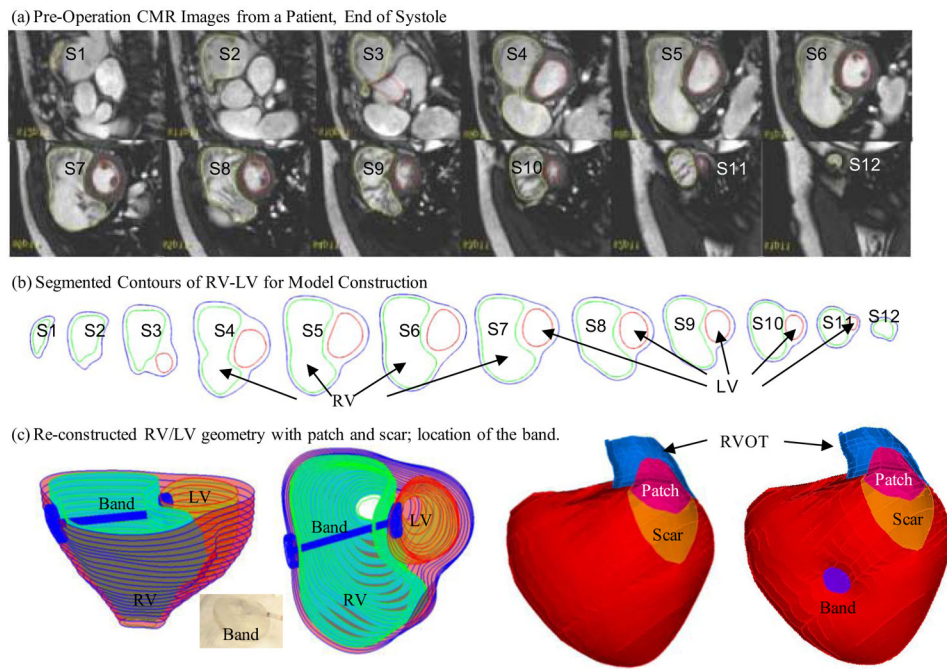


Figure 2. Cardiac MR images of a patient, segmented contours, and reconstructed 3D geometry with and without a band.

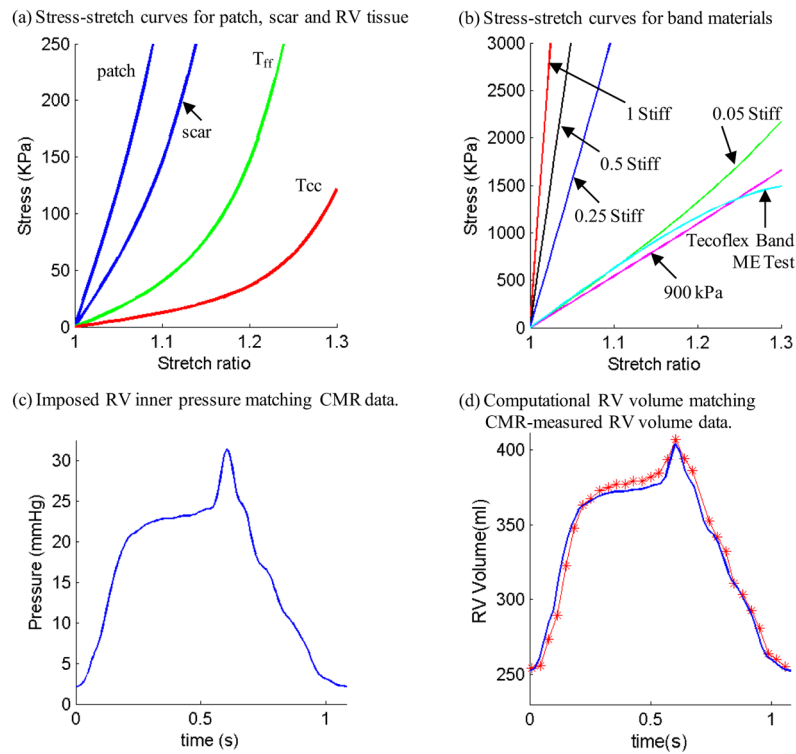


Figure 3. (online only). Material Stress-Stretch curves, pressure conditions used in the paper and computational RV volume curve matching CMR-measured data. (a) Stress-Stretch curves from Mooney-Rivlin isotropic patch, scar and anisotropic RV tissue models used in this paper. Model parameter values ($c_2=0$ for all models): Anisotropic RV model (out-layer given in plot): $c_1=5.746$ kPa, $c_2=0$, $D_1=1.479$ kPa, $D_2=3.0$, $K_1=23.413$ kPa, $K_2=3.2$; Scar: $c_1=19.227$ kPa, $c_2=0$, $D_1=19.227$ kPa, $D_2=9.0$; Patch: $c_1=38.454$ kPa, $c_2=0$, $D_1=38.454$ kPa, $D_2=9.0$; T_{ff} : Stress in the fiber direction; T_{cc} : Stress in fiber circumferential direction. (b) Stress-Stretch curves from Mooney-Rivlin isotropic models for passive band materials. 1 Stiff: $c_1=12,000$ kPa, $D_1=6,000$ kPa, $D_2=1.4$; 0.5 Stiff: $c_1=6,000$ kPa, $D_1=3,000$ kPa, $D_2=1.4$; 0.25 Stiff: $c_1=3,000$ kPa, $D_1=1,500$ kPa, $D_2=1.4$; 0.05 Stiff: $c_1=600$ kPa, $D_1=300$ kPa, $D_2=1.4$; Curve fitting ME testing data: $c_1=1,510$ kPa, $D_1=-221.9$ kPa, $D_2=2.0$; 900 kPa band: $c_1=900$ kPa, $D_1=0$ kPa, $D_2=0$. (c) Imposed inner RV pressure; (d) Model validation: computational RV volume from the baseline no-band model matching CMR-measured RV volume Data.

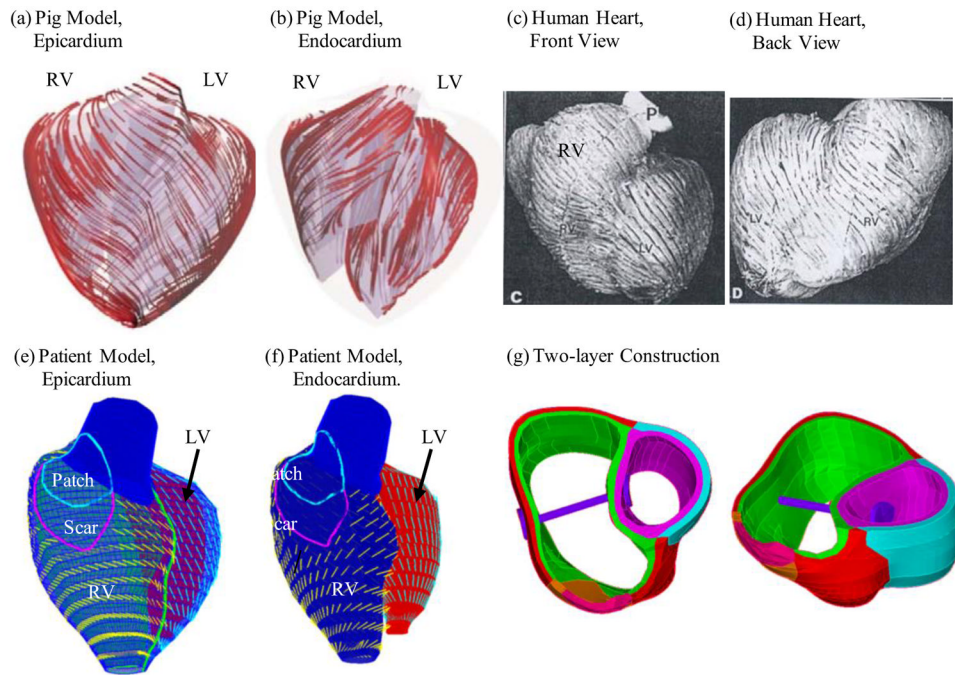


Figure 4. Fiber orientation and two-layer model construction. (a)–(b) Fiber orientations from a pig model (a) on the epicardium, (b) on the endocardial surfaces. LV fiber orientation is approximately -60° (relative to the circumferential direction) at the epicardium, and $+80^\circ$ at the endocardium. (c) Human ventricle fiber orientation from a patient; (d)–(e) Fiber orientation from our proposed RV/LV model based on patient-specific RV/LV morphologies. RV fiber orientation was set -45° at the epicardium, and $+40^\circ$ at the endocardium. The angles can be adjusted to fit patient-specific data. (f) Two-layer model construction illustration using two slices.

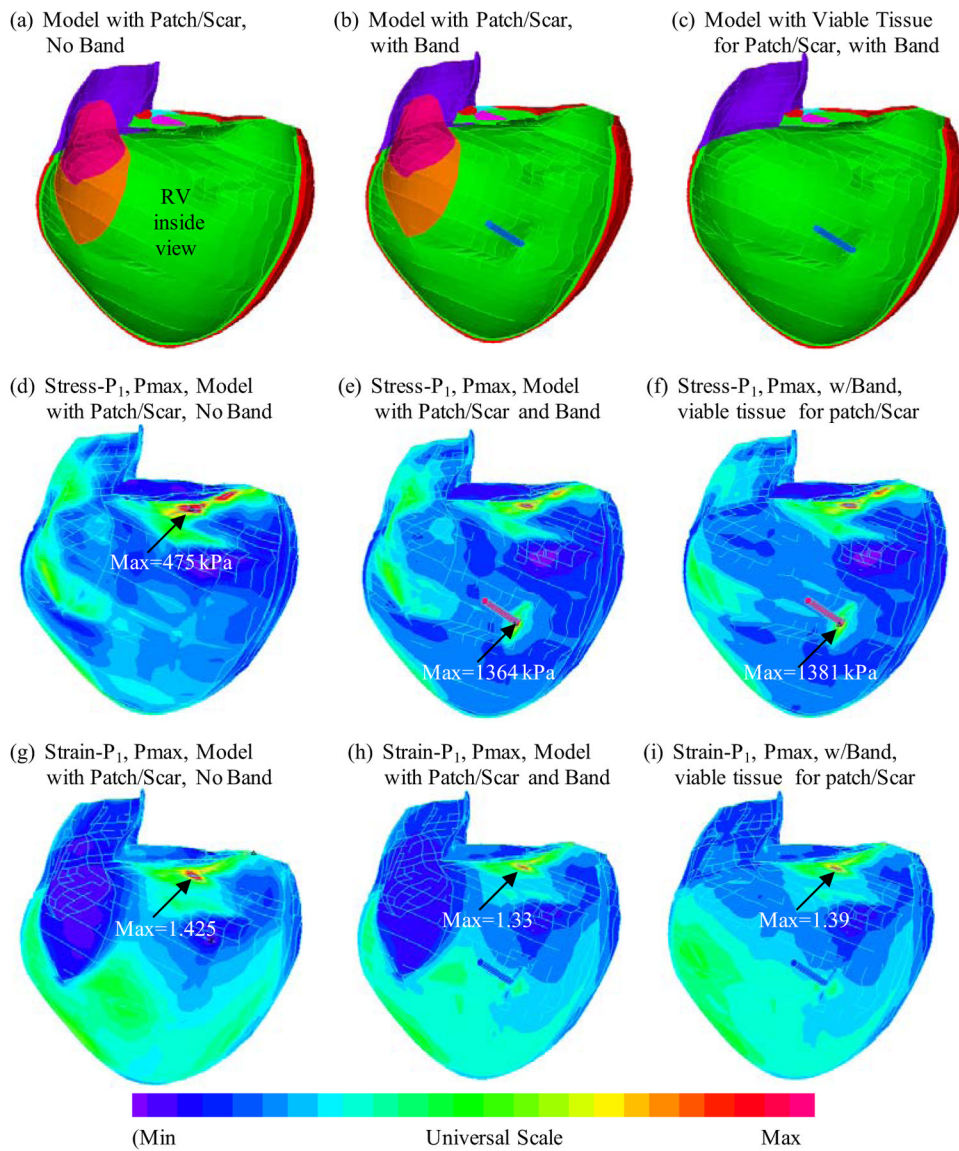


Figure 5. (online only). Stress and strain plots from three models corresponding to maximum pressure condition showing complex stress/strain behaviors.

Table 1

Summary of RV ejection fractions from 12 models with 4 stiffness and 3 band length variations. Softer and longer band provided slightly better ejection fraction. EF rates from all passive band models were 5% lower than the no-band model. Mooney Rivlin model parameters for the 4 band stiffness variations: 1 Stiff: $c_1=12,000$ kPa, $D_1=6,000$ kPa, $D_2=1.4$; 0.5 Stiff: $c_1=6,000$ kPa, $D_1=3,000$ kPa, $D_2=1.4$; 0.25 Stiff: $c_1=3,000$ kPa, $D_1=1,500$ kPa, $D_2=1.4$; 0.05 Stiff: $c_1=600$ kPa, $D_1=300$ kPa, $D_2=1.4$. Band no-load length: 100%: 4.18 cm (the distance between the two locations on the ventricle wall from the no-band model where band would be placed); 90% band length: 3.76 cm; 80% band length: 3.34 cm. PBM: passive band model.

Models	Band Stiffness	Band Length	End of Systole RV Vol (ml)	End of Diastole RV Vol (ml)	EF(%)
CMR Data			254.5	406.9	37.45%
Base Model	N/A	No Band	252.5	403.8	37.48%
PBM1	1	100%	245.9	363.4	32.33%
PBM2	0.5	100%	245.9	364.1	32.47%
PBM3	0.25	100%	246.0	365.6	32.71%
PBM4	0.05	100%	246.4	373.0	33.94%
PBM5	1	90%	240.3	353.8	32.08%
PBM6	0.5	90%	240.3	354.7	32.23%
PBM7	0.25	90%	240.4	356.1	32.49%
PBM8	0.05	90%	240.8	363.8	33.80%
PBM9	1	80%	234.3	344.0	31.87%
PBM10	0.5	80%	234.4	344.7	32.02%
PBM11	0.25	80%	234.4	346.2	32.28%
PBM12	0.05	80%	234.9	354.1	33.67%

Table 2

Summary of RV ejection fractions from 6 active band models compared with their corresponding passive band models. Zero-stress end of systole band length for the passive band model was 4.18 cm. The zero-stress end of systole band length for the active band models with 10%, 15% and 20% active contraction were 3.76, 3.55, and 3.34 cm, respectively. Parameter for band material: $c_1=900$ kPa, $D_1=0$ kPa, $D_2=0$.

Models	Band Active Contraction (BAC)	End of Systole RV Vol (ml)	End of Dystole RV Vol (ml)	EF(%)
Models with Patch and Scar				
Base Model	No Band	252.5	403.8	37.48%
PBM13	Passive	246.4	373.9	34.10%
ABM1	BAC=10%	246.1	393.3	37.43%
ABM2	BAC=15%	237.9	392.6	39.39%
ABM3	BAC=20%	234.1	389.6	39.92%
Models with Patch and Scar Replaced by Normal Tissue				
PBM14	Passive	247.1	383.7	35.59%
ABM4	BAC=10%	246.7	408.1	39.54%
ABM5	BAC=15%	238.6	404.4	40.99%
ABM6	BAC=20%	234.7	402.1	41.63%